ABSTRACT

DEVELOPMENT OF A SPECIFIC-USE POWER CONVERTER TO EFFICIENTLY SUPPLY A MEMS-TYPE ACTUATOR WITH THE ENERGY PRODUCED FROM A GLUCOSE FUEL CELL: *A PRELIMINARY INVESTIGATION INTO THE FUTURE DEVELOPMENT OF AN ARTIFICIAL MUSCLE CELL*

Kurk Macphearson, MS
Department of Electrical Engineering
Northern Illinois University, 2015
Dr. Donald Zinger, Director

The objective of this thesis is to develop a theoretical power converter that is capable of powering a MEMS-type electrostatic microactuator from the power provided by a glucose fuel cell. The proposed converter is to serve as an investigation into the possibility of developing an artificial muscle cell that is able to draw energy directly from the sugar in human blood and convert it into linear motion. The ultimate intent is to develop an actuation approach envisioned to drive active prosthetics that are permanently attached to the human body in the effort to eliminate the need for external power sources.

The final configuration of the power converter is based on a switched capacitor high-ratio step-up converter that is capable of providing a minimum 7.0 volt output while being supplied with 0.75 volts input. The 7.0 volt output limit is determined by a review of literature related to the selected electrostatic microactuator and the 0.75 volt input limit is dictated by reviewed research on glucose fuel cell technologies. The final configuration performs as designed and shows that the concept of using the energy stored in the blood to drive mechanical actuators is achievable and the development of an artificial muscle cell is possible. Furthering this technology could lead to advancements in both active prosthetics and robotics.

NORTHERN ILLINOIS UNIVERSITY
DEKALB, ILLINOIS

AUGUST 2015

DEVELOPMENT OF A SPECIFIC-USE POWER CONVERTER TO EFFICIENTLY SUPPLY A MEMS-TYPE ACTUATOR WITH THE ENERGY PRODUCED FROM A GLUCOSE FUEL CELL:

A PRELIMINARY INVESTIGATION INTO FUTURE DEVELOPMENT OF AN ARTIFICIAL MUSCLE CELL

BY

KURK MACPHEARSON

A THESIS SUBMITTED TO THE GRADUATE SCHOOL

IN PARTIAL FULFILMENT OF THE REQUIREMENTS

FOR THE DEGREE

MASTER OF SCIENCE

DEPARTMENT OF ELECTRICAL ENGINEERING

Thesis Director:
Dr. Donald Zinger

ACKNOWLEDGEMENTS

I would like to thank my primary thesis advisor Dr. Donald Zinger for helping me along the path I have chosen. I am truly grateful for his insight and leadership. I would like to thank Dr. Martin Kocanda for directing me to the answers of so many of my seeming unrelated questions. I would also like to thank Dr. Lichuan Liu and Dr. Michael Haji-Sheikh for agreeing to be my committee members. Thank You.

DEDICATION

To my wife

TABLE OF CONTENTS

LIST OF TABLES

LIST OF FIGURES

CHAPTER 1

INTRODUCTION

1.1 Background

It has been reported in the United States alone that there are approximately 185,000 amputation surgeries performed each year resulting in nearly two million people living their lives as amputees [1]. Although the use of prosthetic devices by these amputees allows for participation in life by providing certain types of ambulation, current prosthetics are considered far less than optimal with regards to the issues of fit, control, and function [2]. To better address these issues a new discipline of active prosthetics called neuroprosthetics has emerged. Neuroprosthetics is a combination of neuroscience and bioengineering aimed at developing prosthetic devices used to replace or improve lost motor and sensory functionality [40]. Many of these neuroprosthetics are powered by an external power source. Active prosthetics that are powered by batteries suffer the same drawbacks of any device powered by batteries which are that the extra batteries add weight and can only provide a limited run time [3].

It is the limitations associated with using external batteries that first fostered the idea of using the energy stored in the human bloodstream to power these advanced prosthetic devices. Abundant empirical evidence is available that demonstrates that there is enough chemical energy within the blood to provide ample power for human ambulation. It seems feasible that if these types of active neuroprosthetics could be supplied by this same chemical power source than there

would be enough energy to provide for adequate ambulation, given that this energy could be converted efficiently. This realization led to the development of the following hypothesis.

The chemical energy stored in the human blood can be a viable source of power sufficient to drive dynamic prosthetics that will one day be permanently attached to an amputee's anatomy eliminating the need for external power sources. Given that the method of conversion from chemical energy to mechanical energy is achieved efficiently.

1.2 Motivation

The motivation for developing the proposed power converter is to initiate the first steps toward realization of a concept of creating a viable and practical artificial muscle cell model that is able to convert the available chemical energy found in the human blood directly to linear mechanical motion similar to a biological muscle cell. A rendering of the artificial muscle cell concept can be seen in Figure 1. The intended purpose of developing the artificial muscle cell is to improve the performance of dynamic human prosthetics. The ultimate objective is to develop an artificial muscle cell that can function as a seamless combination of power supply, converter, and actuator in a single unit. The development of this artificial muscle cell would have profound effects on how future neuroprosthetic devices are designed, constructed, and ultimately used. By eliminating the need for an external power source the weight of the dynamic prosthetic can be minimized allowing for much more efficient prosthetic devices design.

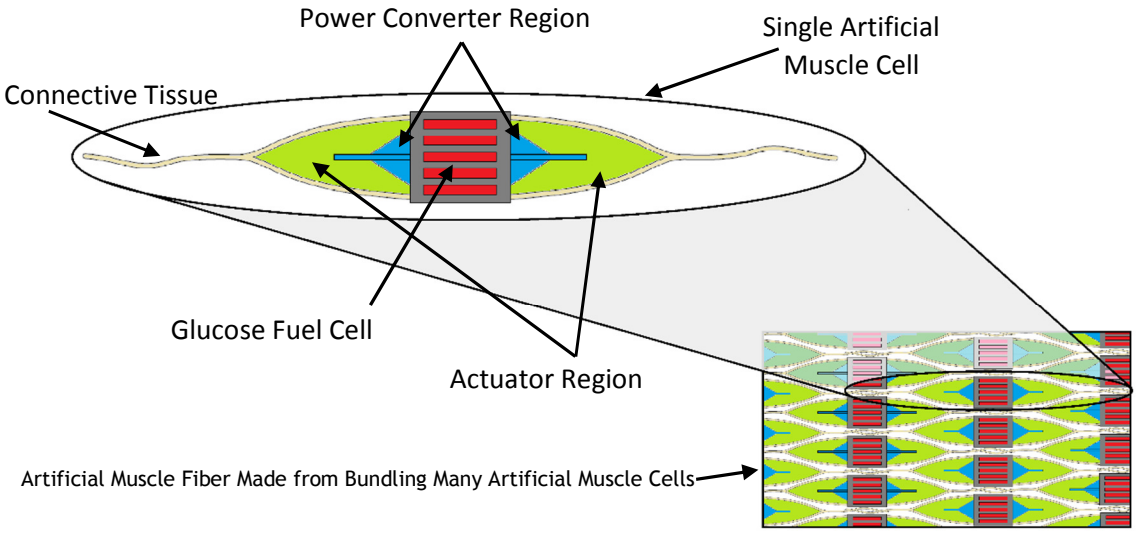

Figure 1 Future artificial muscle cell rendering.

The proposed converter was envisioned as a bridge between two existing technologies. The concept was to investigate the possibility of driving an ideal microactuator from the power provided by a glucose fuel cell. A rendering of the functional position of the proposed power converter can be seen in Figure 2. The following work describes the approach used to determine the required characteristics of the proposed converter and the methods used to simulate the final model.

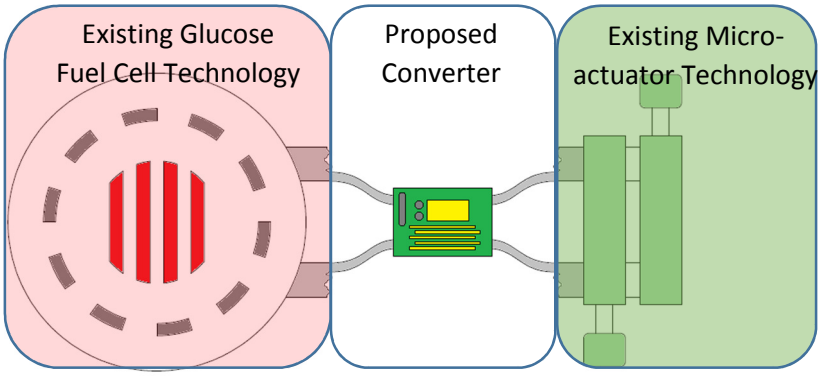

Figure 2 Proposed Converter Functional Position

CHAPTER 2

FUEL CELLS

2.1 Description

As glucose is understood as a universal fuel throughout biology [4] and it is considered the most important simple sugar in human metabolism [5] the first step was to determine the appropriate method of using this simple sugar as the power source for the proposed converter. The most promising technology as a candidate for converting the chemical energy found in glucose to the usable form of electricity is the fuel cell. According to the United States Department of Energy a fuel cell is a device that uses a fuel and oxygen to electrochemically create electricity without employing combustion. The general structural arrangement of a fuel cell consists of an electrolyte material placed between two catalyst-coated electrodes, one electrode serving as the cathode and the other serving as the anode. When fuel is introduced to the device an electrical current is produced and will continue to do so as long as the fuel is being supplied [6].

There are many types of fuel cells in development which are classified by the type of catalyst used within the system [6]. The catalyst within the fuel cell determines many factors about the fuel cell such as the type of fuel that will be used and the chemical reactions that take place. These factors make different fuel cells more suitable for certain applications. Biofuel cells (BFC) or microbial fuel cells (MFC) are a class of fuel cell that incorporates biological organisms in the catalyst material that allows for the utilization of glucose as a preferred fuel

source [6]. This class of fuel cell, referred to as glucose fuel cell, was chosen to provide the input parameters for the proposed converter.

2.2 Candidate Selection

A literature review was conducted to gain a better understanding of the typical output characteristics being reported in the published research on current glucose fuel cell technologies. The data collected from the literature was used to provide a means of benchmarking the devices based on attributes such as power density, the open collector voltage (OCV), and the molar concentration of glucose. These data points along with other information was gathered and can be seen in Table 1.

Table 1 Comparison data.

	Power Density	Current Density	Load	Open Circuit Voltage	Molar Concentration Glucose	Operating Temperature	Effective Electrode Area
Ref-#	mW/cm^2	mA/cm^2	Ω	V	M	°C	cm^2
[7]	0.18	1.68	550k	0.192	0.01	18 -24	0.02
[8]	0.0004	0.03	1000	0.488	0.0042	37	1.2
[9]	0.61	2.13	OC-SC	0.771	0.89	Rm	27
[10]	0.0011	0.01	-	0.218	0.70	37	2.25
[11]	0.58	4.80	Var-Meg	0.230	0.01	37	0.0078
[12]	0.295	1.58	SC	0.625	1.00	23	2.3
[13]	0.036	0.45	Var-Meg	0.420	0.01	-	0.0078
[14]	0.62	5.03	SC	0.644	1.00	Rm	3.8
[15]	0.80	8.00	SC	0.626	1.00	Rm	-
[16]	0.126	1.34	SC	0.425	0.03	Rm	**61.3mm²/g***
[17]	0.0235	-	SC	0.560	0.02	Rm	-
[18]	4.80	20.50**	-	-	0.20	30	5
[19]	0.322	-	SC	-	0.01	50	1
[20]	2.30	8.60	-	0.400	0.50	-	5.67
[21]	0.0162	0.111	54k	0.880	0.05	22	-

** Based on nano-structure, Effective Electrode Area given based on gram weight of material.*
*** Based on graphical interpretation*
SC - Short Circuit, OC - Open Circuit, OC-SC - Load varied from OC to SC, Var-Meg - 1M Ω Potentiometer Varied
Rm - Operational Temperature Declared to be Room Temperature

It was determined that the fuel cell attribute of power density should be used as the limiting value in determining the available voltages and currents to be supplied to the proposed power converter. The attribute of power density is used because this value is able to be used to determine the power that could theoretically be produced by the fuel cells. From this indicated power a voltage value and current value can be established to determine the inputs to the proposed converter. In addition, the power density value can also be used to give an indication of the size of the fuel cell needed to power the proposed converter.

The power densities being achieved by the glucose fuel cells are directly related to the concentration of glucose being supplied to them. The resulting power densities increases proportionately when the concentration of glucose that is supplied to the fuel cells is increased. This increase in power density holds true for supplied concentrations up to a maximum value of about 0.98 M and then starts to decline as the glucose concentration continues to increase [9][22]. Figure 3 and Figure 4 support these findings. Although the reviewed data indicates an upper limit for glucose concentration effects on power density, the challenge for this thesis work is to investigate the power densities at much lower concentrations of glucose.

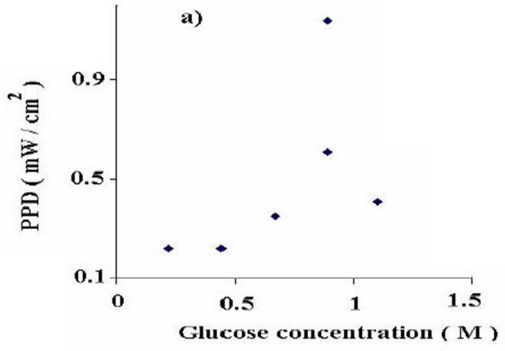

Figure 3. Peak Power Density (a)... as function of $[glu]_0$

Figure 3 Plot of power density vs glucose concentration (Figure 3. from Mor).

Table 1: List of Experiments and singular results.

#	$[glu]_0$ [M]	OCV [V]	PPD [mW/cm^2]	J_{PPD} [mA/cm^2]
1	0.22	0.674	0.22	0.86
2	0.44	0.679	0.22	0.86
3	0.67	0.698	0.35	1.51
4	0.89	0.771	0.61	2.13
5	1.11	0.688	0.41	1.16
6	1.11	0.732	0.42	1.18

Figure 4 Collected data relating power density to glucose concentration (Table 1 from Bubis).

Given that stable concentrations of glucose in the human blood range from approximately 3.9 mM to 5.0 mM [8], it must be noted that the majority of the fuel cells described in the reviewed literature operated at much higher glucose concentrations ranging from about 0.01 M to 1.0 M. In order to derive usable values for power density at the physiological glucose concentrations, extrapolated values are needed. By plotting the pertinent data from the table shown in Figure 4 it is observed that the lowest two data points, the point at 0.22 M glucose and the point at 0.44 M glucose, produce the same power density value of 0.22 mW/cm^2. Based on the available data and by accepting that this data indicates the normal operating conditions of a glucose fuel cell, it is assumed that this system behaves linearly at least at values below a certain glucose concentration threshold. This assumption allows for the linearization around an operation point to be applied thus allowing for the identification of a reasonable fuel cell power density function based on supplied glucose concentrations closer to human physiology.

It is inferred from the data that if the operating point was at 0.22 M glucose then there existed a window extending to the point at 0.44 M glucose in which the system remains linear, see Figure 5. This same window can then be extended in the opposite direction down to the point at 0.00 M describing the same system linearity. The application of this linearization around the chosen operation point provides the tool for ultimately determining the available power that can be supplied to the proposed converter for the simulations. To reiterate, according to this approach, a fuel cell with a known power density that is in operation while being supplied with a glucose concentration of less than 0.44 M can be used to determine a working power density at physiological glucose concentrations.

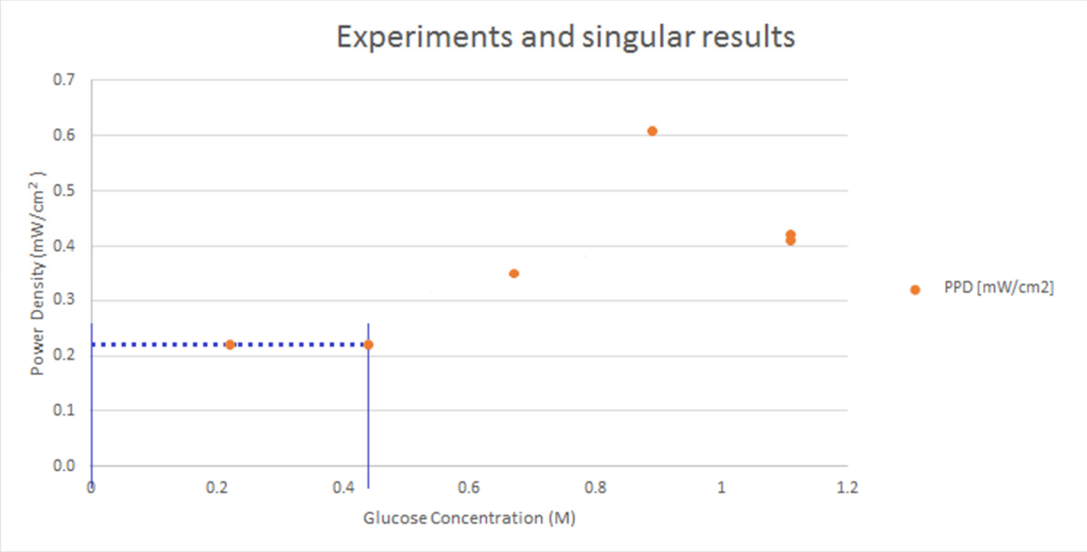

Figure 5 Plot and assumed linearization about the 0.2M glucose operation point.

2.3 Proposed Converter Input Estimations

The voltage and current values used in the simulations are determined based on the working power density identification methods established by the application of the previously discussed linearization techniques. This working power density is based on the highest reported power density of any of the fuel cells found to be operating at a glucose concentration below the 0.44 M concentration limit. A working power density value of 4.8 mW/cm^2 was established and is based on a fuel cell that was being supplied with 0.2 M glucose. This working power density provides a method for determining the theoretical working power available that can be supplied from the glucose fuel cell to the proposed power converter. By dictating the size of the effective electrode area the theoretical working power can be calculated. It is this theoretical working power that is used to ultimately determine the maximum input voltage and input current for the proposed power converter. Although the flexibility of this approach allows for any practical working input voltage to be selected, a voltage of 0.75 volts is selected as an upper end reasonable working voltage based on the open circuit voltages (OCV) reported in the literature.

CHAPTER 3

MICROACTUATORS

3.1 Description

Microactuators are simply actuators that have been developed on the microscopic scale. Where the term microscopic is referred to in the classical sense in that an object of interest is smaller than can be easily seen with the unaided eye. Microactuators make up one of the components studied in an area of technological development referred to as Micro-Electro-Mechanical Systems or MEMS [23]. MEMS are descried as miniaturized mechanical and electro-mechanical elements that are developed using microfabrication techniques [23].

These microactuators perform the same role as standard actuators by providing the means for converting stored energy into a controlled motion which are used in a mechanical system. There are different types of microactuators which are generally classified based on the energy source used to power them and/or the methods used to control them. An electrostatic type microactuator was chosen as the representative load for the proposed power converter because of its small size and because it typically consumes very little power due to their capacitive nature [24]. These types of microactuators rely on exploiting the forces that exist between charged particles to produce movement. One particular example of an electrostatic type microactuator was discovered during the development of this thesis' proposal and has remained the top candidate as the basis for the development of the output parameters that are required by the proposed converter.

3.2 Candidate Selection

The microactuator of interest is described as an electrostatic inchworm type MEMS actuator that was developed in the published article "A Low-Voltage Large-Displacement Large-Force Inchworm Actuator" authored by Mehmet A. Erismis, Herc P. Neves, Robert Puers, and Chris Van Hoof. The authors describe the development of a new family of pull-in style micro actuators with low operational voltages that have the ability to vary the displacement from nanometers to micrometers through minor changes in the design. The authors' main goal for the development of the new actuator type was to address the drawbacks of using current micro actuators for in-vivo biomedical applications due to higher input voltages.

The basic design of the actuator is based on six smaller pull-in actuators arranged in a configuration that allows for the manipulation of a central shuttle. Two of the small pull-in actuators are used to "Drive" the main shuttle back and forth by distorting the angle of a bent beam structure [24] providing the primary displacement of the device. The four remaining pull-in actuators are used to "Latch" the ends of the shuttle to maintain a desired shuttle position [24], as illustrated in Figure 6. When the pull-in actuators are triggered in the correct sequence an overall progression can be achieved by the shuttle allowing for desired displacements of actuation. The authors describe a modified control circuit that supplies positive and negative switching signals used to cancel out any accumulated charges within the actuator which successfully minimized stiction and allowed repeatable operation at frequencies around 75 Hz [24]. These frequencies are considered to be well suited for in vivo biomedical applications [24]. This set up is described as inexpensive and simple to fabricate and has produced working actuators that have reached more than 25 million cycles without significant deterioration in performance [24].

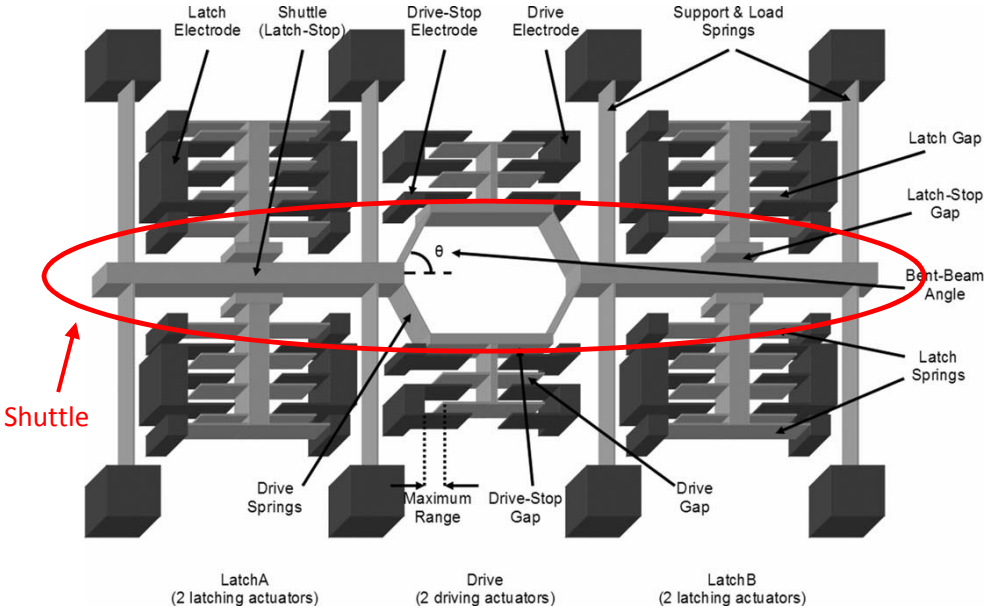

Fig. 2. Schematic view of our inchworm actuator topology. It has four latching and two driving actuators. The drive-stop electrodes prevent total collapsing of the drive actuators during pull-in. The shuttle serves as the stopping electrode for the latching actuators.

Figure 6 Inchworm schematic (Fig. 2 from Erismis).

According to their research the authors believe they have succeeded in developing an actuator with the lowest operational voltage for similar types of hardware. The article describes an actuator driven at reported voltages as low as 7V while being able to provide ±30µN of output force with a total overall displacement of ±18µm [24]. The results of the authors benchmarking studies are displayed in Figure 7 which shows the extremely low operational voltages that were achieved when compared to similar published work. This benchmarking gave compelling evidence that the stated 7 volts was an appropriate target output for the proposed power converter.

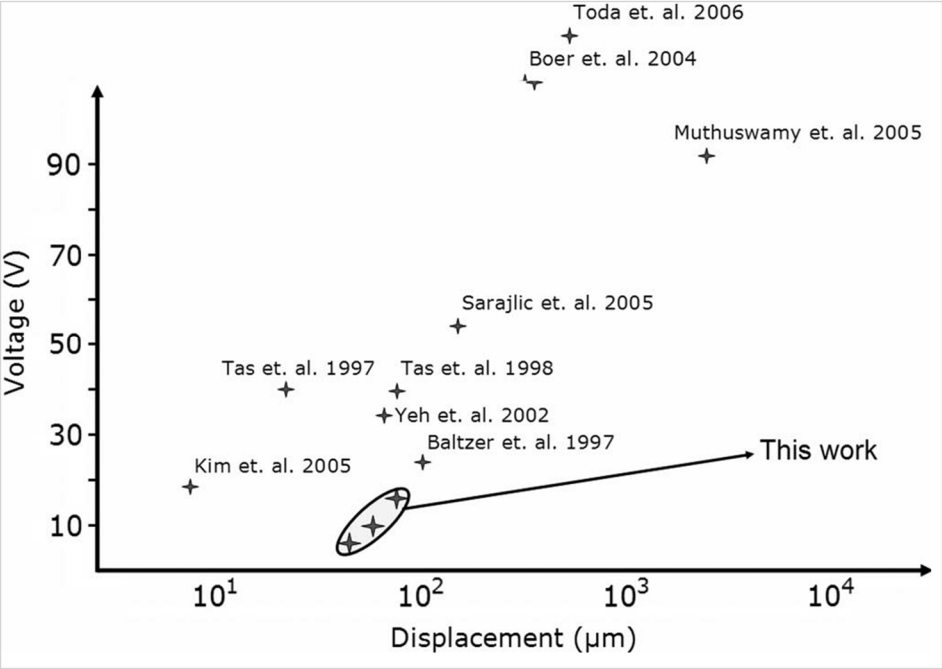

Fig. 1. State-of-the-art benchmarking of inchworm actuators.
Figure 7 Benchmarking of inchworm actuators (Fig. 1. from Erismis).

A second article coauthored in part by the same researchers described the development a similar low voltage microactuator that was referred to as a state-of-the-art low-voltage low-power actuator [27]. The second article titled "Low voltage electrostatic inchworm actuators in aqueous environments," claimed that this type of actuator is low-power and that the device consumes only dynamic power due to its electrostatic nature [27]. This reference to dynamic power consumption implies that the actuator only consumes power when it is in a "pull-in" state and when at rest it theoretically consumes nothing. Based on these claims it has been concluded that for simulation purposes the currents required to drive the electrostatic type microactuator will be mostly related to the minimal leakage currents within a capacitive device.

3.3 Proposed Converter Output Estimations

The low operational voltages achieved by the authors of these articles are seen as the ideal target voltages for the proposed power converter. The 7.0 V operational voltage described in the reviewed literature is the lowest found and is chosen as the target output voltage for the converter simulations. The reviewed literature also referred to a second similar actuator that had been developed that was described as low-power and that it consumed only dynamic power due to its electrostatic nature. The reference to dynamic power consumption implies that the actuator only consumes a very small amount of power when it is in a "pull-in" state and when at rest it theoretically consumes nothing.

CHAPTER 4

PROPOSED CONVERTER

4.1 Design Considerations

The purpose of the following simulations are to develop a power converter that is capable of operating on a minimal amount of input current which is capable of providing an output DC voltage of 7.0 volts while being supplied with an input DC voltage of 0.75 volts. The power converter has the intended use of supplying a MEMS-type electrostatic microactuator with the energy produced from a glucose fuel cell.

One of the main design considerations is overall size reduction. During the simulations the focus is to reduce the size of the proposed power converter while keeping the size of the effective electrode area of glucose fuel cell to a minimum. MEMS-type devices are inherently small, therefore the reported area of 6.66 mm^2 for the electrostatic microactuator serves as the benchmark for size comparisons. While some theoretical exercises are used to reduce the component size of the converter, the main focus is to reduce its current draw of the converter. Reducing the current draw of the converter will reduce the total power consumed by the system. From this reduced power consumptions, a lower power density will be required by the glucose fuel cell which in turn will reduce the required size of its effective electrode area.

Based on the reviewed literature it has been determined that a working power density value for the fuel cells is 4.8 mW/cm^2. With a fixed power density value and by holding the

input voltage to the converter constant the following equation can be used to determine the effective electrode area of the glucose fuel cell required for each simulation.

$$A_{EE} = \frac{V_{in} * I_{iSS}}{4.8\, {}^{mW}/_{cm^2}} \tag{1}$$

Where A_{EE} is the calculated effective electrode area, V_{in} represents the supply voltage of 0.75 V and I_{iSS} is the average steady state current drawn by the converter.

4.2 Initial Simulations

Because the microactuators outlined in the reviewed literature are referred to as electrostatic, a capacitor is used for modeling purposes. The literature describes these microactuators as having a "pull-in" state defined by the equation,

$$V_{pull-in} = \sqrt{\frac{8kd^3}{27\varepsilon A_{cap}}} \tag{2}$$

Where k is the total spring constant, d is the gap between fingers, ε is the permittivity of air, and A_{cap} is the total capacitance area [24]. This equation is of similar form to the equation for calculating the force on an ideal parallel plate capacitor shown as follows,

$$F = \frac{\varepsilon_0 A V^2}{2d^2} \tag{3}$$

Where F is the force generated between the plates, ε_0 is the permittivity of free space, A is the relative area, V is the applied voltage, and d is the average gap between the two parallel plates. This similarity is used to derive a representative capacitance for simulating the inchworm actuator. First the terms are rearranged to find the relative area giving the equation.

$$A = \frac{2Fd^2}{\varepsilon_0 V^2} \tag{4}$$

Next the variables are replaced by the given actuator values where F = 30-μN and V = 7 volts, the appropriate value for the variable d was determined to be the stop gap distance and was stated as 2µm for the drive portion of the actuator [24]. This results in a calculated relative area of 5.50x10^{-7} m^2. This value is used to calculate the capacitance in the following equation.

$$C_{Act} = \frac{\varepsilon_0 A}{d} \tag{5}$$

Resulting in an actuator capacitance of 2.54x10^{-12} farads (C_{Act} = 2.54 pF).

OrCAD Pspice is used to simulate the initial converter concept which is based on a boost converter coupled to a buck converter as shown in Figure 8. The strategy being to first boost the low working voltage supplied by the glucose fuel cell up to a relatively high voltage and then buck the recently boosted voltage back down to the desired operational voltage of the selected electrostatic inchworm microactuator. This topology was originally implemented to provide the maximum available current at the output, but was abandoned as it was discovered that the boost converter alone is capable of supplying adequate current when configured to operate within the desired limits.

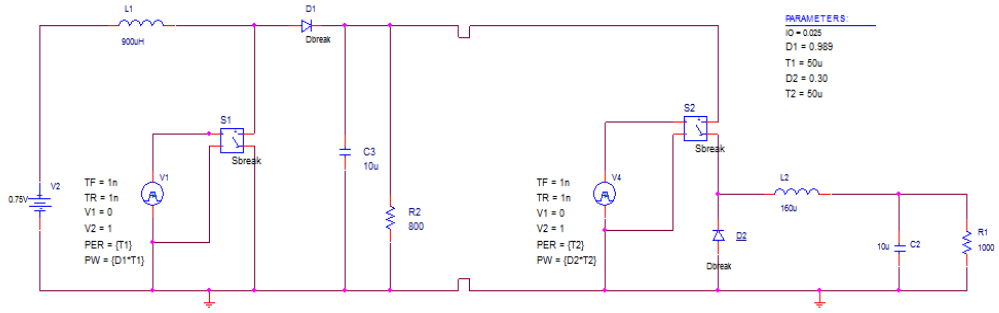

Figure 8 Initial converter topology (Boost - Buck).

4.3 Standard Boost Converter Simulations

A standard boost converter is simulated after the buck converter portion was removed from the initial topology. This greatly simplifies the process for determining the ideal converter attributes, such as duty cycle and inductor value, by allowing the standard formulas to be used. To calculate the duty cycle (D) for the boost converter the following equation is used,

$$D = 1 - {}^{V_{in}}/_{V_{out}} \qquad (V_{out} > V_{in}), \tag{6}$$

Where V_{in} and V_{out} are chosen to be 0.75 volts and 7 volts respectively resulting in a duty cycle of $D = 0.893$. This value is used to calculate the optimal inductor size for the converter based on a switching frequency (f_S) of 20 kHz and an initial current ripple (I_{ripple}) of 20 mA. The following equation is used where $T_S = 1/f_S$ resulting in an inductor value (L) of 1.674 mH.

$$L = {}^{(V_{in} * D * T_s)}\Big/_{I_{ripple}} \tag{7}$$

The switching frequency and the current ripple values are selected as reasonable starting points for the simulation process along with the initial load resistor value of 1 kΩ and the output filter capacitor value of 10 uF. Figure 9 shows the completed boost converter modeled in Orcad Pspice and Figure 10 shows the resulting outputs which correspond to these estimated values. The resulting output voltage is approximately 6.994 volts and the ripple present in the inductor current is about 19.983 mA with a steady state maximum current of approximately 75.284 mA.

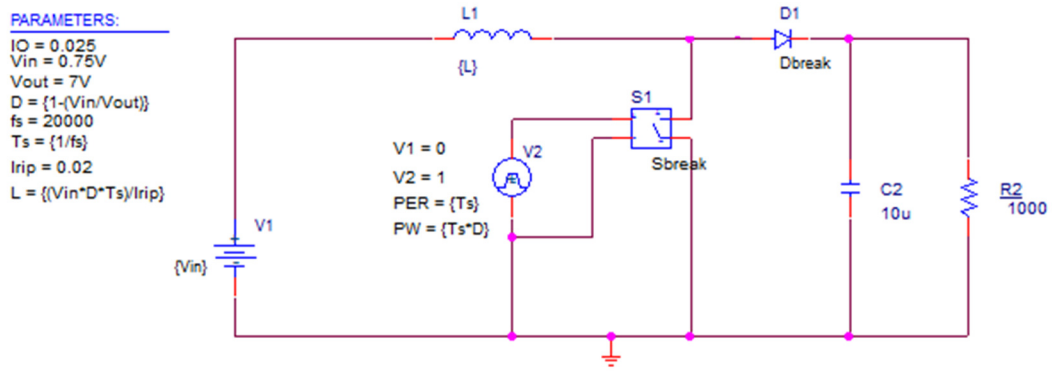

Figure 9 Initial boost converter topology.

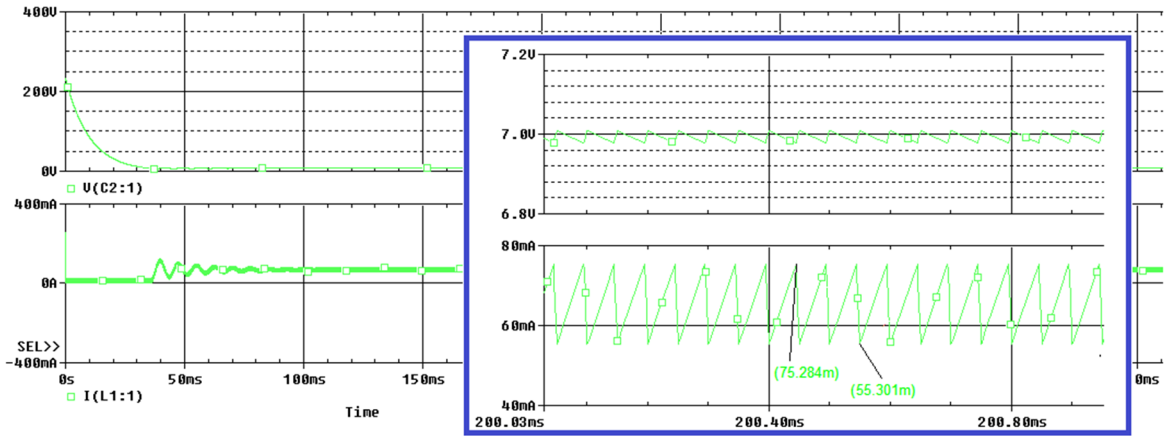

Figure 10 Initial boost converter outputs.

Next a 2.54 pF capacitor calculated to represent the electrostatic inchworm microactuator is added to the load side of the converter, shown in Figure 11, and the simulations are again performed with the results shown in Figure 12. As is expected, applying the additional small capacitor for the actuator in parallel with the much larger filter capacitor does not change the output values significantly. See Table 2 found on pg. 20. The resulting steady state maximum inductor current for the new configuration is about 75.281 mA. In this boost converter topology the current through the inductor is equal to the input current drawn by the converter. With the input voltage selected to be 0.75 volts and an input current of 75.281 mA the input power can be roughly calculated to be 56.463 mW. The resulting effective electrode area is 11.763 cm^2 based on the previously determined fuel cell power density of 4.8 mW/cm^2. This estimated area is

significantly larger than the given area of the actuator which is approximately 6.66 mm^2. Given that the required size of the fuel cell is directly related to the current drawn in by the converter, the next step is to reduce the current being used by the converter. This is achieved by optimizing the passive components of the boost converter.

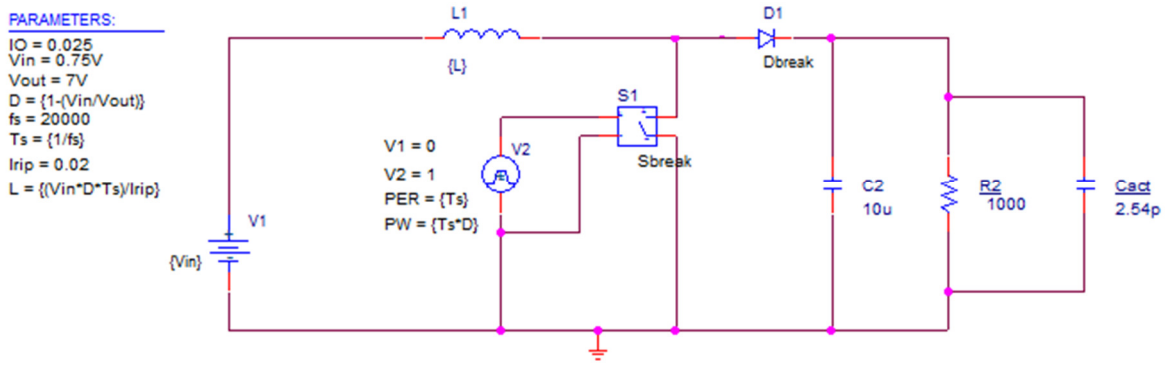

Figure 11 Boost converter topology with actuator capacitance added.

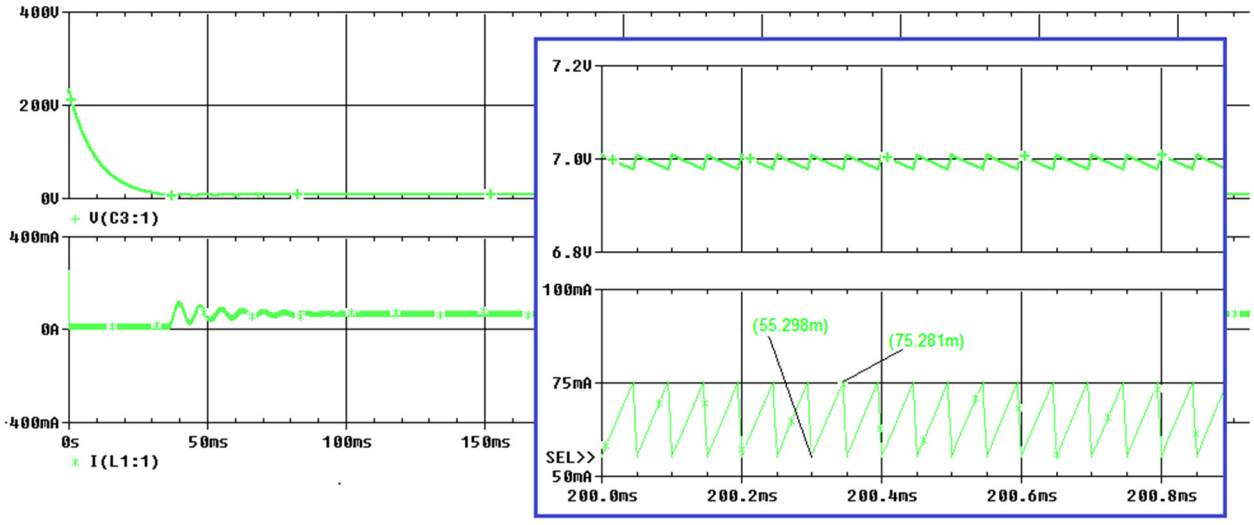

Figure 12 Boost converter output with actuator capacitance added.

Table 2 Boost converter behavior before and after applied actuator capacitance.

Table 2			
Steady State		W/o C_{act}	W/ C_{act}
mA	IL_{ripple} Max	75.284	75.281
	IL_{ripple} Min	55.301	55.298
	IL_{ripple}	19.983	19.983
V	VC_{ripple} Max	7.0093	7.0093
	VC_{ripple} Min	6.9781	6.9781
	VC_{ripple} Max	0.0312	0.0312

As the power into the converter is equal to the power out of the converter, minus some losses, the first place to attempt to reduce the power consumed by the converter is to reduce the power output by the converter. With the output voltage of the boost converter set to the required minimum voltage of 7.0 volts the best option reducing the power is to reduce the current through the load resistor (R2) that is fixed across the converters output. This is done by increasing the resistance of R2. The largest practical resistor value that can be used that allows the converter to remain in continuous conduction mode (CCM) is the described as the critical resistance R_{crit}, and is defined by the equation,

$$R_{crit} = \frac{2Lf_S}{D(1-D)^2} \tag{8}$$

This equation results in a calculated critical resistance value of 6533.33 Ω for the current configuration of the boost converter. As expected, when this value is used for the load resistance in the simulation it does not cause the converter to operate in discontinuous conduction mode (DCM).

To determine the critical load that will actually cause the boost converter simulation to go into DCM a method of trial and error is used. Starting with the calculated R_{crit} value the load resistance is incremented through successive iterations until the critical simulation resistance

value (R_{Scrit}) is established. This approach determines R_{Scrit} to be 6931.87 Ω resulting in a six percent increase in the resistance required to cause the boost converter to go from CCM into DCM. Figure 13 shows the comparison of the inductor currents from the simulations for the two different load resistor values. The steady state inductor current remains positive for the calculated R_{crit} value indicating CCM operation and remains negative for the established R_{Scrit} value indicating DCM operation.

To push the limits of the boost converter a load resistance that is just slightly less than a resistance that causes a DCM condition needs to be employed. Based on the determination of the two previous resistance values maximum load resistance (R_L) is established. In an effort to have the converter safely remain in CCM it is determined that a load resistance that is approximately 10% less than the R_{Scrit} value will be used. This R_L value happens to be about 5% less than the calculated R_{crit} value, therefore for simulation purposes, the scaling factor $R_L = 0.95(R_{crit})$ is used giving a load resistance of 6206.67 Ω.

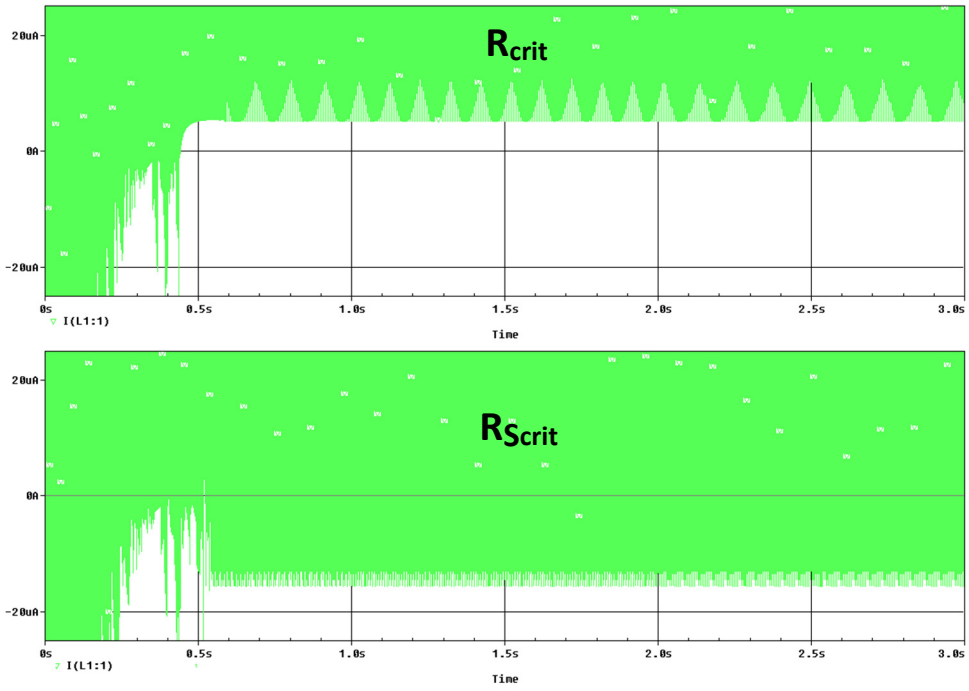

Figure 13 Calculated critical resistance vs simulated critical resistance.

Running the simulation with the established theoretical minimum load reveals a new steady state maximum current of about 20.532 mA. Based on the 0.75 V input voltage and the fuel cell power density of 4.8 mW/cm^2 this indicates a new effective electrode area for the fuel cell that is calculated to be about 3.208 cm^2. This is a size reduction of almost 400% but is still not significant enough to bring it down to a size that is comparable to the nominal size of the electrostatic inchworm microactuator.

To reduce the power consumed by the boost converter even more the maximum steady state current drawn in from the glucose fuel cell is reduced. This is a two-step approach. First, a steady state maximum current is determined by dictating the required effective electrode area. By selecting the required effective electrode area size to be the same as the 6.66 m^2 area of the electrostatic actuator a much lower maximum steady state current of 0.425 mA is determined. The 0.425 mA current is determined by the following equation.

$$I_{mss} = \frac{A_{ee} D_P}{V_{in}} \tag{9}$$

Where I_{mss} is the maximum steady state current, A_{ee} is the effective electrode area of the fuel cell, and D_P is the power density of the fuel cell.

Next, the magnitude of the current ripple through the inductor is reduced. With the desired maximum steady state current and the ideal load resistance determined the simulation is conducted once again and successfully produces the desired output voltage of just over seven volts while remaining in CCM. The simulation results shows an average maximum steady state current of about 0.445 mA with a current ripple of about 0.428 mA at steady state. The resulting topology shown in Figure 14 with the archived outputs shown in Figure 15. Forcing the current ripple down to this low value results in an increase in the size of the inductor required for the

boost converter to achieve the desired I_{mss}. Based on Equation 7 the inductor value that this configuration requires is approximately 78.78 mH.

It is difficult to determine the physical size of an inductor based on inductance alone due to other limiting factor such as the core material, coil and wire diameter, and the form factor. Therefore as sizing methodology is adopted to aid in determining component footprint areas. This methodology is to use the footprint area of a commercially available device found to have the same functional characteristics of the component in question. This commercially available device is used as a stand-in device and provides the means of estimating components footprint areas for sizing comparisons.

An estimated size was based on a stand-in part found through a component search for an 80 mH fixed inductor. The PE-51688 from Pulse Electronics Corporation is described as having the dimensions 17.01 mm by 9.91 mm with a height of 20.32 mm [25]. As the literature for either the actuator or the fuel cell do not describe a volume measurement for the components of interest it is assumed that each of these parts has a height associate with the given areas. This assumption is based on the belief that any of the unindicated heights are within a reasonable proportion of the indicated lengths and widths i.e. of the same order of magnitude. Based on this assumption the given areas have been used as a reasonable indication of the overall sizes for the components being described. Therefore, by focusing on only the cross sectional area of the stand-in inductor (168.56 mm^2) it is still much larger than the 6.66 mm^2 established area for the actuator and fuel cell electrode. In an effort to get a comparable inductor size the switching frequency of the converter was investigated.

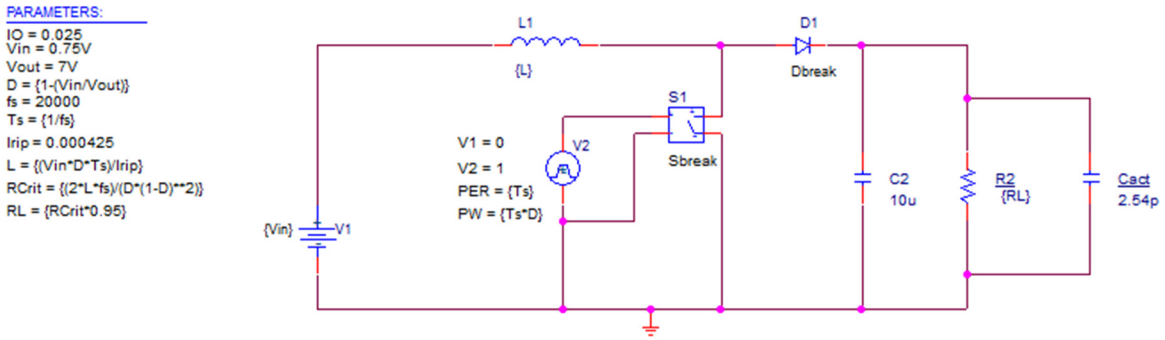

Figure 14 Boost converter topology optimized for minimal fuel cell effective electrode area.

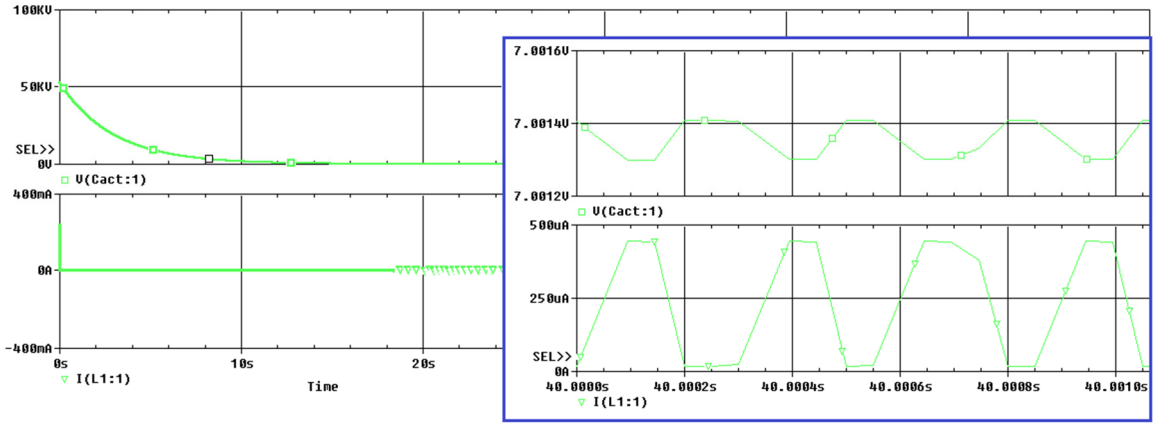

Figure 15 Output from optimized boost converter simulation.

It was determined that by selecting a representative inductor based on its size could provide a method for calculating the target inductance to be used for the simulations. A second stand-in inductor was found based on its area of 6.75 mm^2. The T1008-8R2G fixed inductance device from Tamura was of the right size and had a stated inductance of 8.2 µH [26]. A switching frequency of 19.2 MHz was calculated by the following equation and used for the next set of simulations.

$$f_S = \frac{V_{in}D}{LI_{ripple}} \tag{10}$$

This final configuration for the boost converter performed as designed with an achieved output voltage of approximately 7.0001 V with a inductor current ripple of about 0.436 mA and an average steady state current (I_{LSS}) of about 515.729 µA. The values for the final configuration of the boost converter components can be seen in Table 3.

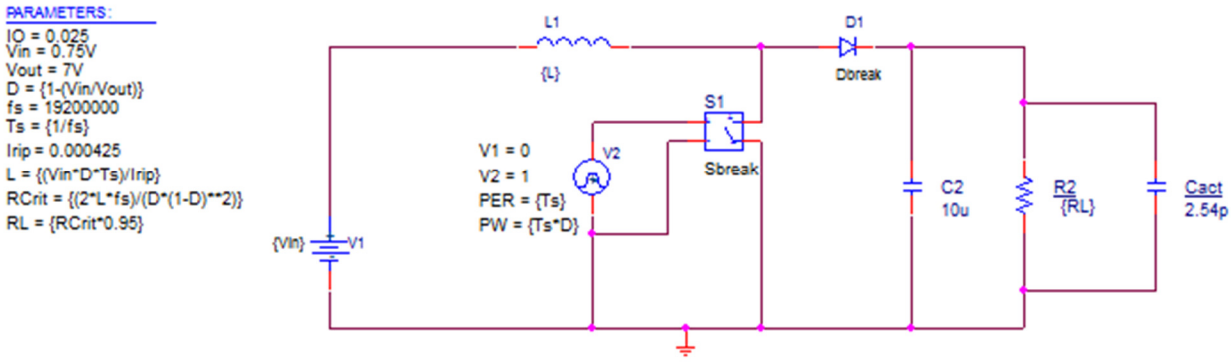

Figure 16 Boost converter topology for final configuration with reduced inductor and increased switching frequency.

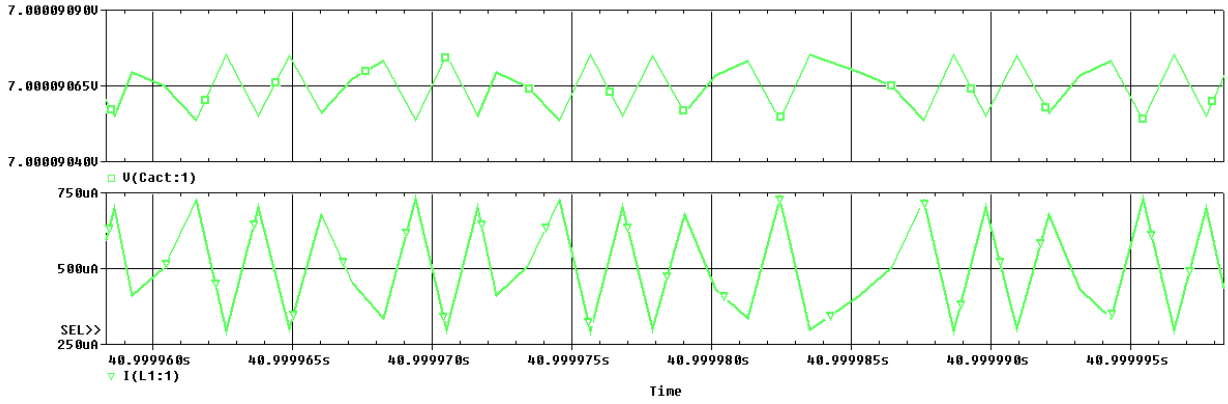

Figure 17 Steady state output from final boost converter with an 8.2 µH inductor switched at 19.2 MHz.

Table 3 Boost converter final configuration.

Table 3		
	Calculated	Simulated
V_{in}	0.75 V	0.75 V
V_{out}	7.0 V	7.0001 V
IL_{ripple}	425 µA	436 µA
f_S	19.2 MHz	19.2 MHz
D	0.893	0.893
L	0.82 µH	0.82 µH
R_L	292 kΩ	292 kΩ

The final configuration of the boost converter, see Figure 16, has a simulated average steady state input current draw of 515.729 µA, shown in Figure 17. According to Equation 1 this input current requires the glucose fuel cell to have an effective electrode area of 8.06 mm^2. One major shortcoming of this model is the rather large representative footprint area of the stand-in inductor determined by the T1008-8R2G fixed inductance device from Tamura. Although the inductor is just one passive component of the boost converter it has an area of 6.75 mm^2 [26] which is slightly larger than the 6.66 mm^2 representative area of the electrostatic microactuator [27].

To establish a conservative but realistic relative area for the other components of the boost converter such as the switch, the diode, the capacitor, and the load resistor a stand-in device is again used. A micro processing unit (MCU) has been selected to account for the area of the rest of the boost converters structure as the typical MCU is able to incorporate many of these components in a single device. MCUs incorporate millions of transistors which are used as oscillators and switches as well as resistors, diodes, and capacitors into a single device with a very small area [28]. The stand-in microprocessor is the Kinetis KL02 microcontroller

developed by Freescale which has a footprint 2.0 mm by 1.9 mm. With an area of 3.80 mm^2, it is the smallest integrated circuit of its kind identified [29]. Because the final configuration of the boost converter contains only one each of the elemental components as opposed to millions, this stand-in was believed to more than adequately represent their cumulative areas along with any wires or bussing structures.

Based on the relative areas of key components for the final boost converter configuration along with the key components of the proposed artificial muscle cell a theoretical sizing scale is determined. A suitable layout can be seen in Figure 18 and is based on the areas of the stand-in devices and the calculated effective electrode area of the fuel cell, the dimensions are given in Table 4.

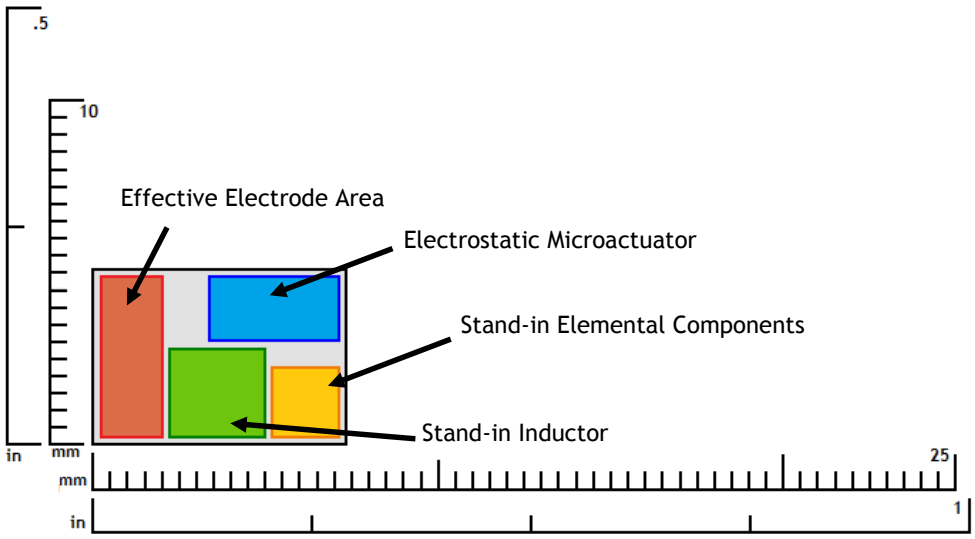

Figure 18 Theoretical sizing scale for the standard boost converter.

Table 4 Boost converter key component dimensions.

Table 4			
Key Component	Length (mm)	Width (mm)	Area (mm^2)
Fuel Cell Effective Electrode	4.60	1.75	8.06
Electrostatic Actuator	3.70	1.80	6.66
Inductor*	2.70	2.50	6.75
Elemental Components**	2.00	1.90	3.80
Total Estimated Area - A_{Total}			25.27

*Based on the T1008-8R2G fixed inductance device from Tamura.
**Based on the Kinetis KL02 microcontroller developed by Freescale.

4.4 Switched Capacitor Converter Simulations

In an attempt to reduce the current required by the system a switched capacitor converter is investigated. This type of converter can be implemented without any inductors or resistors and is based on an interconnected matrix of switches and capacitors that exploits the effects of moving a stored charge between capacitors in a process called charge pumping [30]. Depending on the number of capacitors, the configuration, and the switching sequence almost any ratio of input voltage to output voltage can be achieved [30] providing either buck or boost capabilities. A non-inverting boost configuration called a voltage doubler is employed. The voltage doubler implemented in the simulations uses a switching sequence that alternates the capacitor matrix between a parallel input configuration and a series output configuration shown in Figure 19.

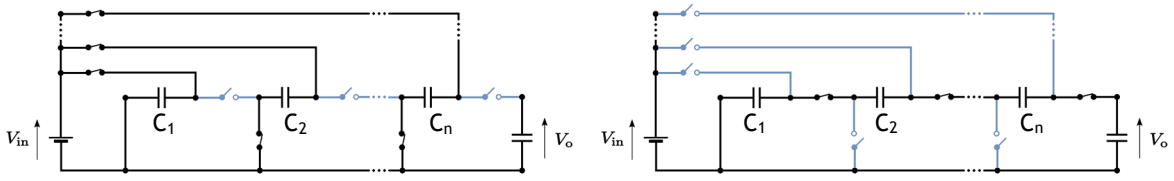

Parallel input configuration

Series output configuration

Figure 19 Switched capacitor boost converter.

This configuration has been selected because it is a high-ratio step-up converter typically used in low power applications and when it is implemented with *n* matched capacitors the approximate output voltage can be estimated using the following formula [30].

$$V_{out} = nV_{in} \tag{11}$$

With the input voltage to the switched capacitor converter fixed at 0.75 V by the glucose fuel cell and the required minimum output voltage of 7.0 V set by the electrostatic microactuator, the previous equation give a resulting *n* of 9.333. Therefore a minimum of ten matched capacitors is required in order to provide the necessary step-up ratio.

OrCAD Pspice is also used to simulate the switched capacitor converter. Figure 20 shows the basic configuration of the Pspice model with the ten matched capacitors and a fixed 2.54 pF capacitor representing the electrostatic microactuator. The basic model also employs a switching scheme that provides a parallel input configuration and a series output configuration. Two different models of the switched capacitor converter are used to investigate functionality and to provide a method for comparing against the standard boost converter previously discussed. The different switched capacitor converter models are referred to as Model-1 and Model-2 for the remainder of the simulations.

Model-1 is set up with a fixed matched capacitors value. With the matched capacitors values fixed the switching frequency used to alter the series and parallel capacitor configurations is varied through a range of different frequencies. Any reasonable value of capacitance could be used for the matched capacitors value, but ultimately a value of 2.54 pF is selected. Based on the electrostatic microactuator this value is selected for simplicity.

Model-2 is alternatively set up to operate at a fixed switching frequency with the matched capacitors value being manipulated for each simulation. Although the fixed variable of switching frequency could be any value, for continuity it is selected based on a previously determined value. The switching frequency for Model-2 was set to the 19.2 MHz switching frequency calculated for the final configuration of the previously modeled standard boost converter.

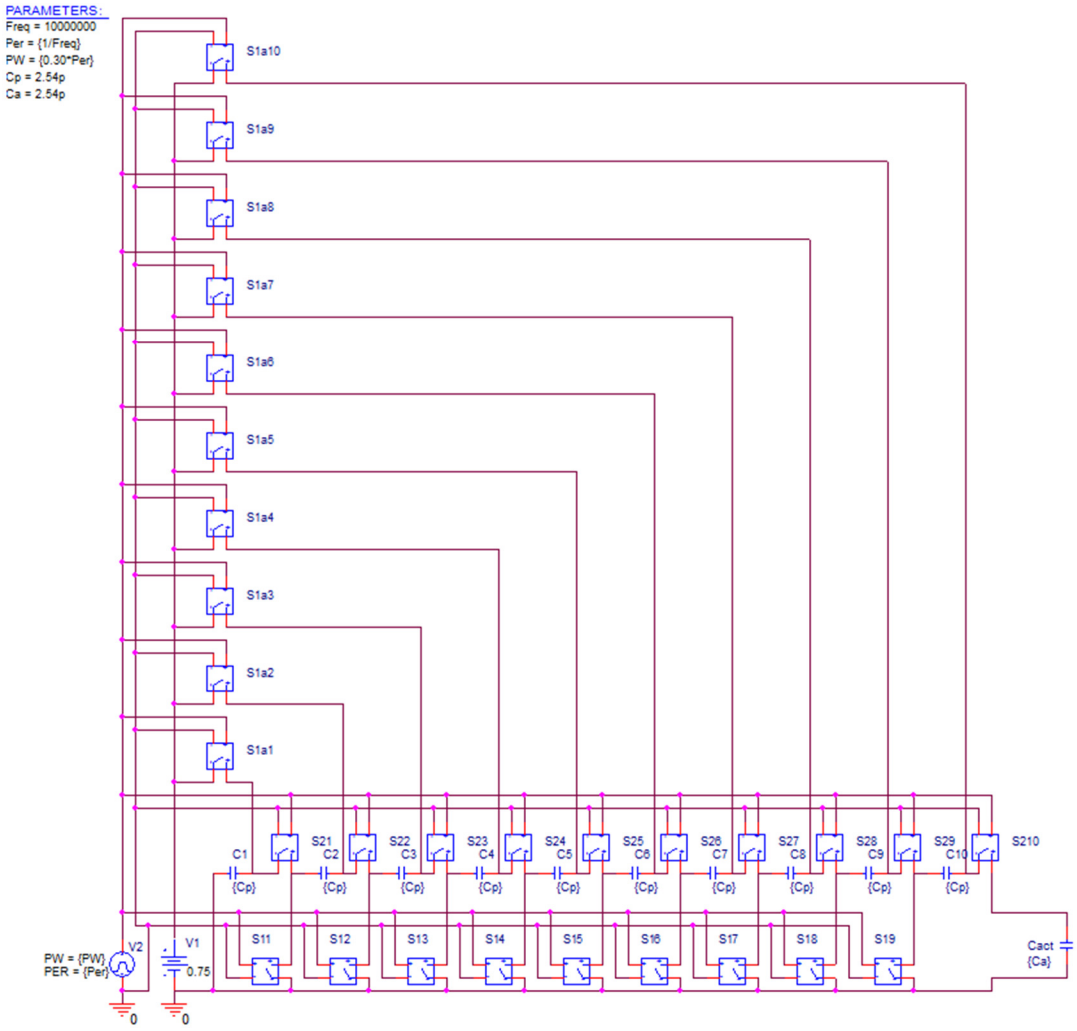

Figure 20 Switched capacitor converter topology with 10 matched capacitors.

4.4.1 Model-1

The Model-1 simulations shows that in order to reach the minimum output voltage of seven volts a switching frequency greater than 0.1 GHz must be used. To be thorough the switching frequency is varied form 0.1 GHz to 1 GHz and the appropriate data is collected. That data is related to the output voltage across the 2.54 pF actuator capacitor and the current drawn in from the voltage source V1. In Figure 21 the average steady state values for the input current and the output voltages are plotted at each of the given switching frequencies.

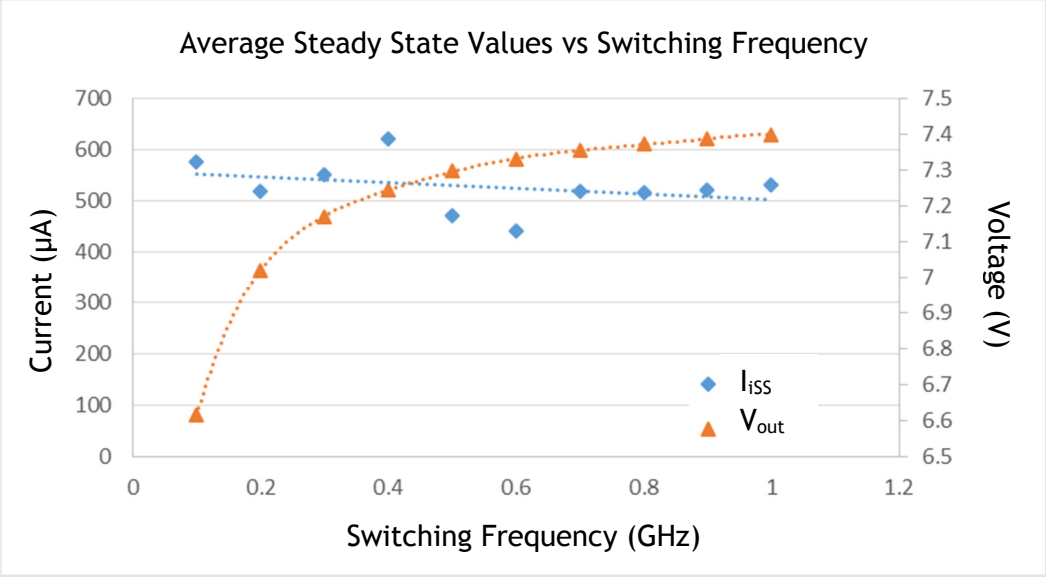

Figure 21 Average steady state values vs. switching frequency Model-1.

The plot shows that the output voltage appears to approach a value less than the 7.5 volts predicted by Equation 11. This is considered reasonable as the formula does not take in to account any considerations for efficiency. This plot indicates that the minimum output voltage is achievable for a switching frequency greater than 0.1 GHz. The steady state current however, is slightly more erratic but has a slight lowering trend as the switching frequency is increased.

To calculate a theoretical pull-in force for the actuator capacitor placed across the output of Model-1 the equation for force on a parallel plate capacitor is used.

$$F = \frac{\varepsilon_0 A V^2}{2d^2} \tag{12}$$

Where F is the force generated between the plates, ε_0 is the permittivity of free space, A is the relative area of the representative capacitor, V is the applied voltage, and d is the 2μm gap specified for the electrostatic microactuator. The previously conducted simulations for the standard boost converter yielded the 2.54 pF capacitor value used to represent the capacitance of the electrostatic microactuator along with that representative capacitor's area of 5.50×10^{-7} m^2. The theoretical pull-in forces related to the achieved voltages are calculated and plotted. By rearranging the terms in Equation 9 the required effective electrode areas can be calculated. These calculated values based on the simulated steady state currents at the corresponding switching frequencies are also plotted. Figure 22 shows these plotted values. When the plot in Figure 22 is compared to the plot in Figure 21 the plots looked identical with the exception of a scale change. This stands to reason as the effective electrode area values and the theoretical pull-in forces are proportional to the input current values and proportional to the square of the output voltage values respectively.

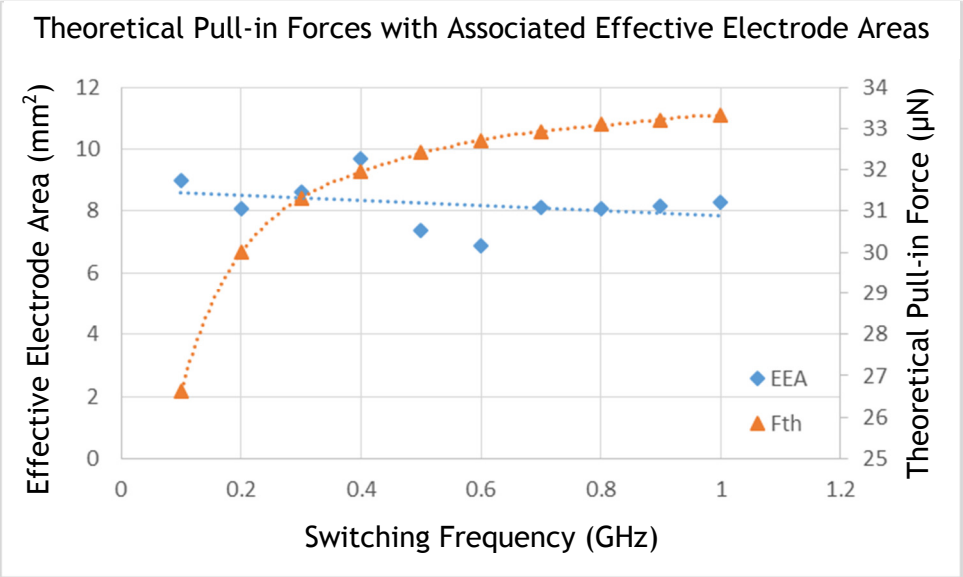

Figure 22 Calculated theoretical pull-in forces and calculated effective electrode areas.

The data portrayed in Figure 22 suggests that there is a diminishing return on an increased switching frequency as both the theoretical pull-in force and the required effective electrode area show a leveling off trend as the frequency is increased. Based on the plot of the theoretical pull in force the optimal switching speed for this model is selected to be at about 0.5 GHz which gave a force of 32.41 µN with an output voltage of 7.2962 V. Because the data for the effective electrode area is more inconclusive the data point at 0.5 GHz will not be used for determining the final effective electrode size instead and average of the areas over the span of frequencies will be determined. This average area is calculated to be 8.23 mm^2 and is used for determining the theoretical size for comparisons.

As with the standard boost converter a theoretical sizing scale is established for Model-1. The sizing scale is based on the calculated effective electrode area and the relative areas of the other key components. The calculated effective electrode area required for Model-1 is slightly larger than the effective electrode area required by the final configuration of the standard boost

converter, but unlike the standard boost converter model the area associated with the stand-in inductor was eliminated resulting in an overall reduction in total estimated area. It is assumed that the stand-in elemental components area is still valid as eleven capacitors and twenty nine switches used in this model are still significantly less than the millions contained in a typical MCU. The new layout shown in Figure 23 depicts the smaller total area with the associated dimensions given in Table 5.

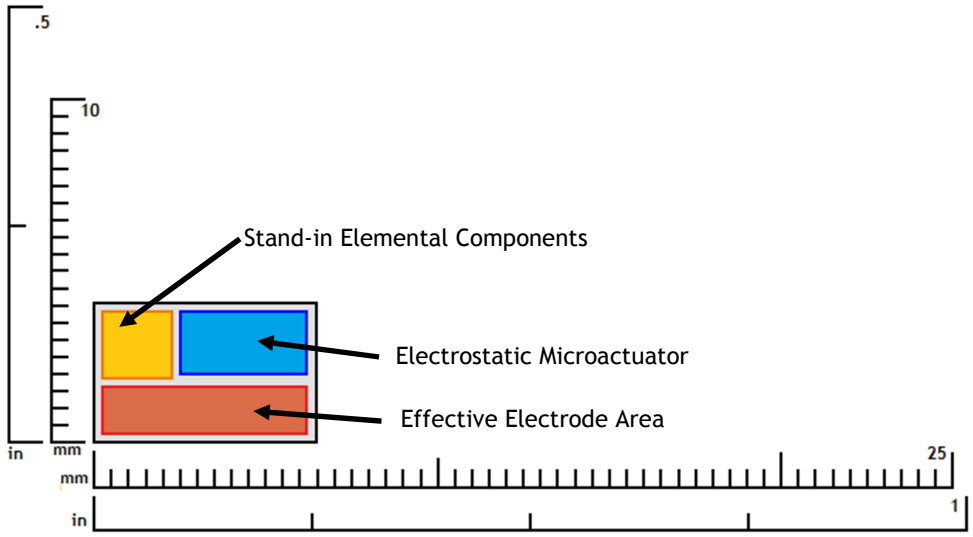

Figure 23 Theoretical sizing scale for the switched capacitor converter Model-1.

Table 5 Switched capacitor converter Model-1 key component dimensions.

Table 5			
Key Component	Length (mm)	Width (mm)	Area (mm^2)
Fuel Cell Effective Electrode	6.01	1.37	8.23
Electrostatic Actuator	3.70	1.80	6.66
Elemental Components**	2.00	1.90	3.80
Total Estimated Area - A_{Total}			18.69

**Based on the Kinetis KL02 microcontroller developed by Freescale.

4.4.2 Model-2

Similar to Model-1 the initial simulations of Model-2 indicate that in order to supply the required 7.0 V minimum output voltage the variable component, in this case the matched capacitors value, has a minimum threshold. This configuration requires a matched capacitors value greater than 25 pF. Again, to be thorough, the simulations are conducted by varying the capacitance from 25 pF to 1 µF and the steady state output voltage and the steady state input current data is collected. This collected data is plotted and shown in Figure 24.

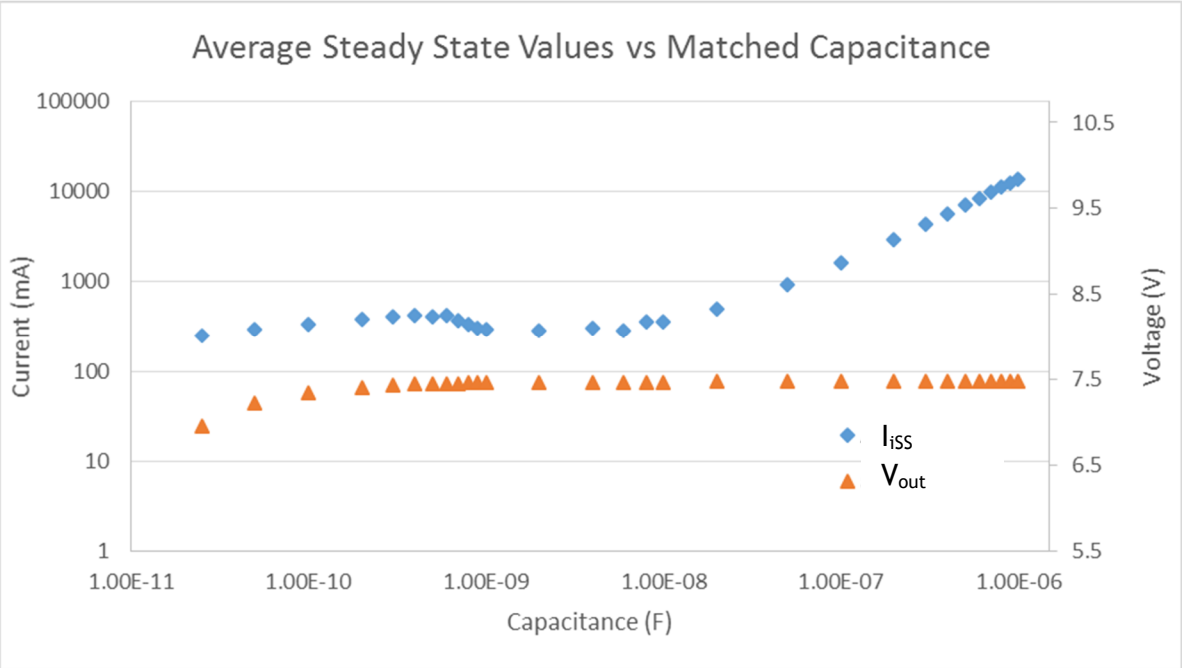

Figure 24 Average steady state values vs. matched capacitance Model-2.

Like Model-1 the output voltage data from Model-2 appears to approach a value slightly less than the predicted 7.5 volts. Unlike Model-1, the steady state input current values behave much more predictively and provide a much clearer indication of the optimal configuration for

Model-2. As was previously established the values collected for steady state input current and steady state output voltage directly indicate the effective electrode size and the theoretical pull-in force respectively. Therefore based on the plot shown in Figure 24 an optimal capacitance value of 2 nF can be established. This capacitance value allows the converter to provide an output voltage of 7.4683 V resulting in a theoretical pull-in force of 33.95 µN. This is achieved while drawing a current of 284.763 µA which indicates a required effective electrode area of 4.45 mm^2. Model-2 has the smallest theoretical sizing scale of all three converter models. Its layout can be seen in Figure 25 with the final dimensions listed in Table 6.

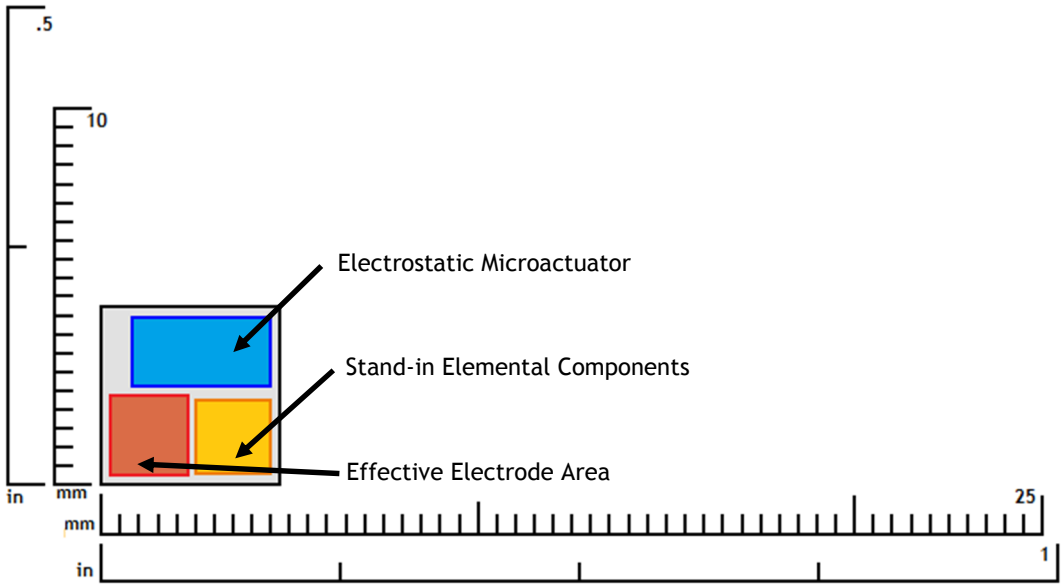

Figure 25 Theoretical sizing scale for the switched capacitor converter Model-2.

Table 6 Switched capacitor converter Model-2 key component dimensions.

Table 6			
Key Component	Length (mm)	Width (mm)	Area (mm^2)
Fuel Cell Effective Electrode	2.13	2.13	4.54
Electrostatic Actuator	3.70	1.80	6.66
Elemental Components**	2.00	1.90	3.80
Total Estimated Area - A_{Total}			15.00

**Based on the Kinetis KL02 microcontroller developed by Freescale.

4.5 Findings

Table 7 shows the final attributes of the three converter models, all three of the converters are capable of providing the minimum 7.0 V output voltage required by the electrostatic microactuator while being supplied by the 0.75 V input voltage provided by the glucose fuel cell. The highest output voltage recorded is from Model-2. This indicates that this converter also has the highest calculated pull-in force which was determined to be 33.95 µN. While the theoretical sizing scale for each of the models can be brought down to relatively small sizes, the final displacement of the effective electrode area for the switched capacitor converter Model-2 is half the size of both the standard boost converter and Model-1. The size comparisons can be seen in Figure 26. Model-2 has the smallest total estimated area of just 15.00 mm^2. This miniature size is owed equally to the absence of an inductor and to the reduction in effective electrode area.

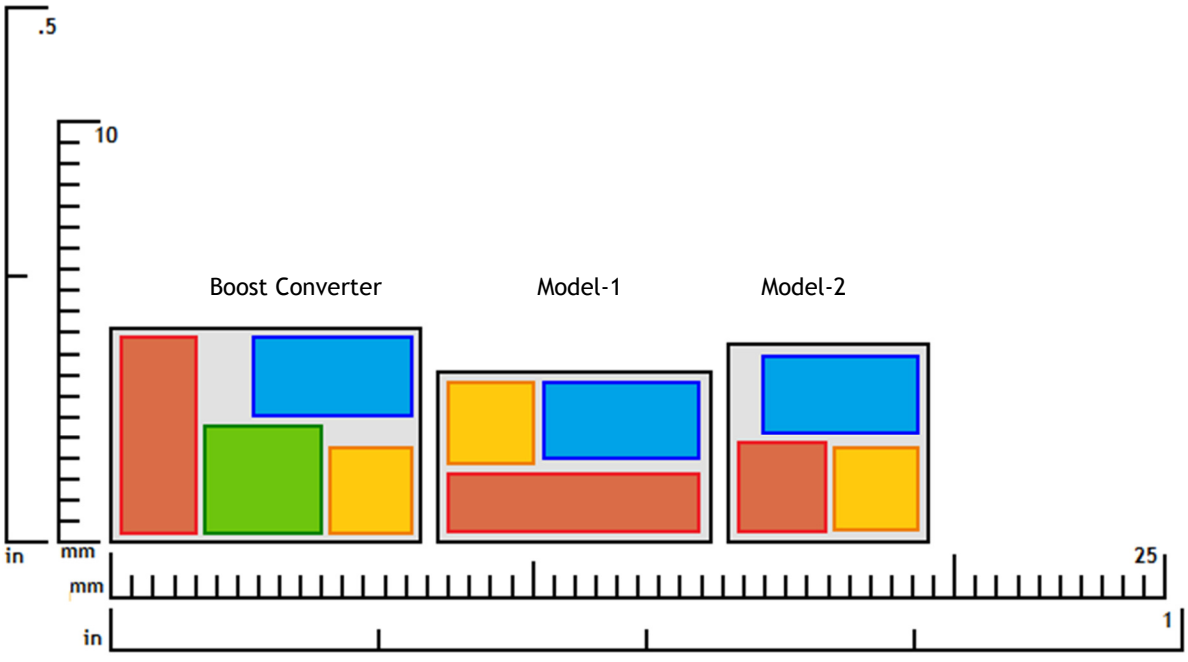

Figure 26 Theoretical sizing scale comparison.

Table 7 Converter models attributes comparison.

Table 7						
	V_{in} (V)	I_{iSS} (µA)	A_{EE} (mm^2)	A_{Total} (mm^2)	V_{out} (V)	F_{pull} (µN)
Boost	0.75	515.729	8.06	25.27	7.0000	29.83
Model-1	0.75	526.531	8.23	18.69	7.2962	32.74
Model-2	0.75	284.763	4.45	15.00	7.4863	33.95

CHAPTER 5

CONCLUSION AND FUTURE SCOPE

5.1 Conclusion

The standard boost converter and the two configurations of the switched capacitor converter that were investigated perform as designed. Each of these converters are able to provide power to the electrostatic micro actuator from the energy supplied by a glucose fuel cell operating at stable human blood glucose concentrations. The switched capacitor converter Model-2 however has the best performance characteristics of the three converters developed.

Model-2 has the highest output voltage which provides the highest pull-in force by the electrostatic microactuator. In addition Model-2 is capable of supplying this output while drawing the lowest input current recorded leading to the smallest required effective electrode area of the supplying glucose fuel cell. Model-2 also had the smallest theoretical sizing scale with a required effective electrode area that was half the area of required effective electrode areas of both the standard boost converter and the switched capacitor converter Model-1.

The preceding work shows that the approach of using the energy stored in the blood to provide mechanical actuation for permanent active prosthetics in humans is a viable concept. It is believed that the development of artificial muscle cell based on a similar configuration to the proposed design of a glucose fuel cell supplying a MEMS-type electrostatic microactuator via a switched capacitor power converter is possible.

5.2 Future Scope

5.2.1 Concept 1

Because both the converter and the microactuator are essentially comprised of capacitive elements it only seems natural within the context of the artificial muscle cell concept that the two technologies could be combined into a single device. By replacing one of the capacitors in the switched capacitor converter with the capacitance of the electrostatic microactuator a resulting novel actuator/power converter hybrid concept can be imagined. This concept is depicted in Figure 27. This could provide an elegant method for reducing size and the component count in the final device and could allow for the implementation of simpler control theories. Combining these into a single device eliminates the need for a separate control scheme for the actuator portion as is intrinsically handled by the control scheme for the switching of the power conversion portion of the hybrid. By manipulating the switching scheme the voltage across the actuator capacitor will be varied which ultimately causes movement in the actuator.

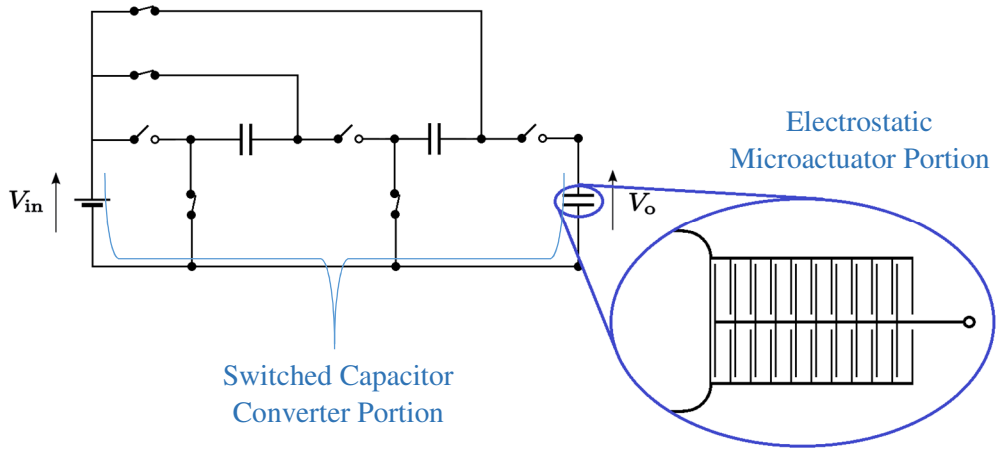

Figure 27 Novel actuator/power converter hybrid concept.

This design could also be improved by having multiple capacitors within the converter being replaced with electrostatic actuators which could potentially increase the “pull-in force” in

one direction of actuation. Furthermore, if the group of electrostatic actuators are placed at predetermined angles to each other controlled multidirectional movements could be obtained.

5.2.2 Concept 2

The artificial muscle concept will also be advantageous for traditional robotics applications. As with active prosthetics for humans removing any external power sources could lead to more compact forms of actuation and could lead to an overall reduction in size and weight. Another major benefit of this concept is that each artificial muscle cell is able to draw energy directly from its environment which eliminates the need to bus power from a separate source to the actuator. This can lead to greater efficiencies by eliminating the losses associated with power transmission through wires and connectors. In addition when applied to traditional robotics the artificial muscle cells and the fuel supplying them will not be limited by such low concentrations of glucose and can be optimized to generate greater amounts of power.

REFERENCES

[1] Ziegler-Graham, K., MacKenzie, E. J., Epharaim, P. L., Travison, T. G., & Brookmeyer, R. (2008).*Estimating the prevalence of limb loss in the united states*. Retrieved from http://www.amputee-coalition.org/limb-loss-resource-center/resources-by-topic/limb-loss-statistics/limb-loss-statistics/

[2] McGimpsey, G., & Bradford, T. C. (n.d.). *Limb prosthetics services and devices critical unmet need: Market analysis white paper.* Retrieved from http://www.nist.gov/tip/wp/pswp/upload/239_limb_prosthetics_services_devices.pdf

[3] Bowker, J. H., & American Academy of Orthopaedic Surgeons. (1992). Atlas of limb prosthetics: Surgical, prosthetic, and rehabilitation principles. Retrieved from http://www.oandplibrary.org/alp/chap34-03.asp

[4] Nakamura, S. (2013). *Handbook of H+ -ATPases*. Boca Raton, FL: CRC Pres.

[5] Georgia Tech University. (2005). Sugars. Retrieved from http://hyperphysics.phy-astr.gsu.edu/hbase/organic/sugar.html

[6] Department of Energy. (n.d.). Fuel Cells. Retrieved from http://energy.gov/eere/fuelcells/fuel-cells

[7] Rapoport, B. I., Kedzierski, J. T., & Sarpeshkar, R. (2012). A glucose fuel cell for implantable brain–machine interfaces. *PLoS ONE, 7,* e38436. doi:10.1371/journal.pone.0038436

[8] Siu, C. -P. B., & Chiao, M. (2008). A microfabricated PDMS microbial fuel cell. *Journal of Microelectromechanical Systems, 17,* 1329-1341. doi:10.1109/JMEMS.2008.2006816

[9] Bubis, E., Mor, L., Kaufman, V., Schechner, P., & Hemmes, K. (2004). *Saccharide fuel cells with platinum particles anode.* Paper presented at the 23rd IEEE Convention of Electrical and Electronics Engineers in Israel, Tel-Aviv, Israel. doi:10.1109/EEEI.2004.1361163

[10] Kerzenmacher, S., Sumbharaju, R., Ducree, J., Zengerle, R., & Von Stetten, F. (2007). *A surface mountable glucose fuel cell for medical implants.* Paper presented at the TRANSDUCERS 2007 - 2007 International Solid-State Sensors, Actuators and Microsystems Conference, Lyon, France. doi:10.1109/SENSOR.2007.4300087

[11] Ammam, M., & Fransaer, J. (2014). Microbiofuel cell powered by glucose/O2 based on electrodeposition of enzyme, conducting polymer and redox mediators. Part II: Influence of the electropolymerized monomer on the output power density and stability. *Electrochimica Acta, 121,* 83-92. doi:10.1016/j.electacta.2013.12.129

[12] Chen, J., Zhao, C. X., Zhi, M. M., Wang, K., Deng, L., & Xu, G. (2012). Alkaline direct oxidation glucose fuel cell system using silver/nickel foams as electrodes. *Electrochimica Acta, 66,* 133-138. doi:10.1016/j.electacta.2012.01.071

[13] Ammam, M., & Fransaer,Y. (2012). Glucose oxidase and 1-butyl-3-methylimidazolium deposited by AC-electrophoresis on Pt as a glucose bioanode for biofuel cells. *Electrochimica Acta, 81,* 129-137. doi:10.1016/j.electacta.2012.07.084

[14] Liu, X., Hao, M., Feng, M., Zhang, L., Zhao, Y., Du, X., & Wang, G. (2013). A One-compartment direct glucose alkaline fuel cell with methyl viologen as electron mediator. *Applied Energy, 106,* 176-183. doi:10.1016/j.apenergy.2013.01.073

[15] Eustis, R., Tsang, T. M., Yang, B., Scott, D., & Liaw, B. Y. (2014). Seeking effective dyes for a mediated glucose–air alkaline battery/fuel cell. *Journal of Power Sources, 248,* 1133-1140. doi:10.1016/j.jpowsour.2013.10.022

[16] Yang, L., Zhang, Y., Chu, M., Deng, W., Tan, Y., Ma, M., Su, X., Xie, Q., & Yao, S. (2014). Facile fabrication of network film electrodes with ultrathin Au nanowires for nonenzymatic glucose sensing and glucose/O2 fuel cell. *Biosensors and Bioelectronics, 52,* 105-110. doi:10.1016/j.bios.2013.08.038

[17] Kilic, M. S., Korkut, S., Hazer, B., & Erhan, E. (2014). Development and operation of gold and cobalt oxide nanoparticles containing polypropylene based enzymatic fuel cell for renewable fuels. *Biosensors and Bioelectronics, 61,* 500-505. doi:10.1016/j.bios.2014.05.068

[18] Basu, D., Sood, S., & Basu, S. (2013). Performance comparison of Pt–Au/C and Pt–Bi/C anode catalysts in batch and continuous direct glucose alkaline fuel cell. *Chemical Engineering Journal, 228,* 867-870. doi:10.1016/j.cej.2013.05.049

[19] Zhu, Z., Sun, F., Zhang, X., & Zhang, Y. -H. P. (2012). Deep oxidation of glucose in enzymatic fuel cells through a synthetic enzymatic pathway containing a cascade of two thermostable dehydrogenases. *Biosensors and Bioelectronics, 36,* 110-115. doi:10.1016/j.bios.2012.04.001

[20] Elouarzaki, K., Haddad, R., Holzinger, M., Le Goff, A., Thery, J., & Cosnier, S. (2014). MWCNT-supported phthalocyanine cobalt as air-breathing cathodic catalyst in glucose/O2 fuel cells. *Journal of Power Sources, 255,* 24-28. doi:10.1016/j.jpowsour.2013.12.109

[21] Slaughter, G., & Sunday, J. (2014). A membraneless single compartment abiotic glucose fuel cell. *Journal of Power Sources, 261,* 332-336. doi:10.1016/j.jpowsour.2014.03.090

[22] Mor, L., Bubis, E., Hemmes, K., & Schechner, P. (2004). *Performance of a glucose AFC.* Paper presented at the Proceedings of the 2004 11th IEEE International Conference on Electronics, Circuits and Systems, 2004. ICECS 2004., Tel Aviv, Israel. doi:10.1109/ICECS.2004.1399672

[23] MEMSnet. (n.d.). What is MEMS technology. Retrieved from https://www.memsnet.org/about/what-is.html

[24] Erismis, M. A., Neves, H. P., Puers, R., & Van Hoof, C. (2008). A low-voltage large-displacement large-force inchworm actuator. *Journal of Microelectromechanical Systems, 17,* 1294-1301. doi:10.1109/JMEMS.2008.2004852

[25] PE-51688. (n.d.). In *Product Data Sheet.* Retrieved from http://productfinder.pulseeng.com/products/datasheets/P578.pdf

[26] T1008-8R2G (n.d.). In *Product Data Sheet* Retrieved from http://media.digikey.com/pdf/Data%20Sheets/Tamura%20PDFs/T1008%20Series.pdf

[27] Erismis, M. A., Neves, H. P., De Moor, P., Van Hoof, C., & Puers, R. (2009). Low voltage electrostatic inchworm actuators in aqueous environments. *Procedia Chemistry, 1,* 686-689. doi:10.1016/j.proche.2009.07.171

[28] Microprocessor. (2000). In *Microsoft Encarta Online Encyclopedia 2000.* Retrieved from http://autocww.colorado.edu/~flc/E64ContentFiles/ComputersElectronics/Microprocessor.html

[29] KinetisKL02. (n.d.). In *Product Data Sheet.* Retrieved from http://www.mouser.com/pdfdocs/KINETISKL02CSPFS.PDF

[30] Krein, P. T. (2015). *Elements of power electronics*. (2nd ed.). New York: Oxford University Press.